

Supporting Information

Multi-channel exciton dissociation in the D18/Y6 complexes for high-efficiency organic photovoltaics

Zhixing Cao,^{a#} Shu Yang,^{a#} Bo Wang,^a Xingxing Shen,^{a,*} Guangchao Han,^b Yuanping Yi^{b,*}

^aCollege of Chemical Engineering, Hebei Normal University of Science & Technology, Qinhuangdao 066004, China

^bBeijing National Laboratory for Molecular Sciences, CAS Key Laboratory of Organic Solids, Institute of Chemistry, Chinese Academy of Sciences, Beijing 100190, China

Contents

Figure S1. Optimized S_0 geometries for one repeating units of D18, and Y6 with whole alkyls

Figure S2. HOMO and LUMO for one, two and three repeating units of D18.

Figure S3. Optimized S_0 geometries for two repeating units of D18, and Y6 with methyl.

Figure S4. Initial intermolecular configuration for the D18/Y6 complex.

Figure S5. Optimized geometries of the S_0 , S_1 and cationic states for D18.

Figure S6. Energy differences between the configurations derived from translation and rotation of Y6 and optimized configuration.

Figure S7. Calculated energies of the CT states for the D18/Y6 complex.

Figure S8. Gibbs free energies for the exciton dissociation and charge-recombination processes.

Figure S9. Evolution of exciton-dissociation rates from the S_1 state of D18 to the CT_0 state.

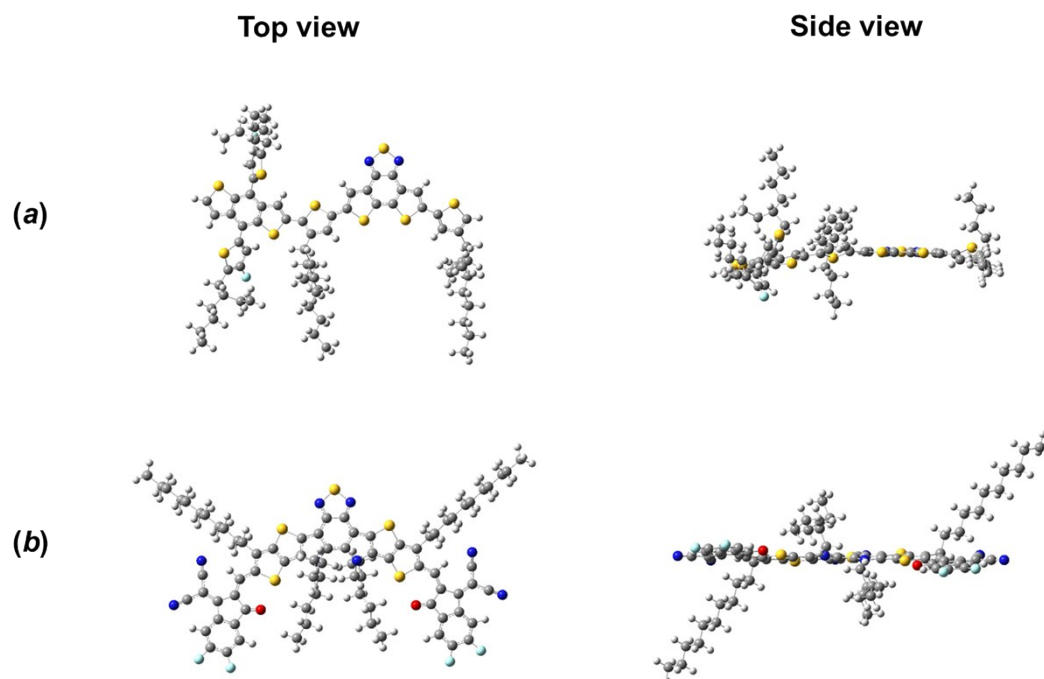


Figure S1. Optimized ground geometries for (a) one repeating unit of D18 and (b) Y6 containing whole alkyl groups.

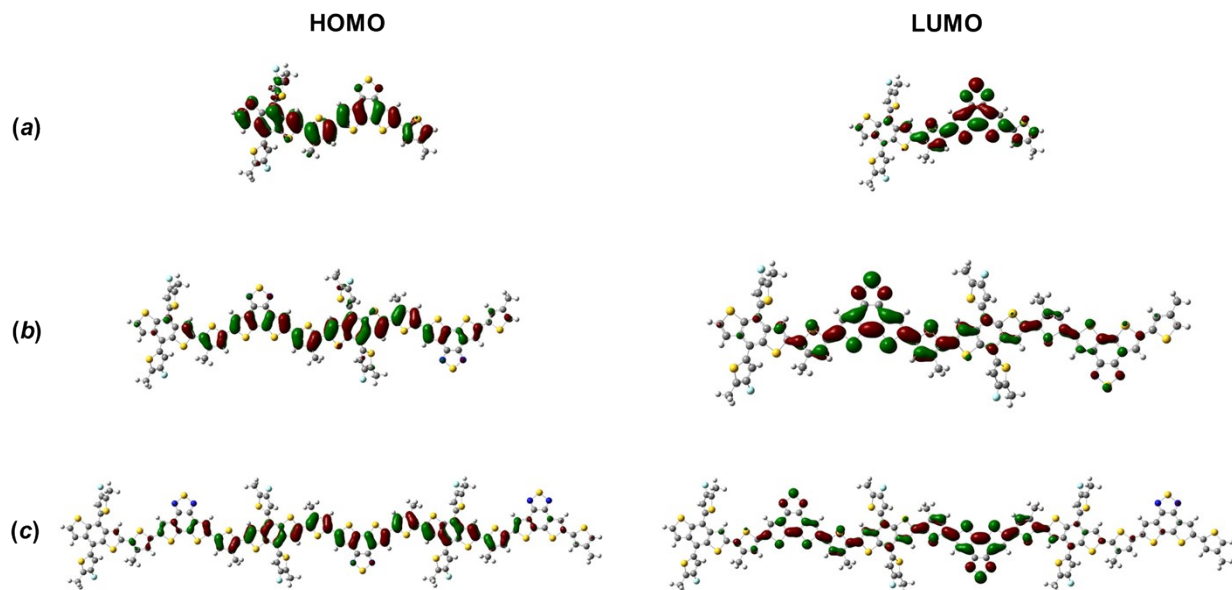


Figure S2. HOMO and LUMO for (a) one repeating unit, (b) two repeating units, (c) three repeating units of D18.

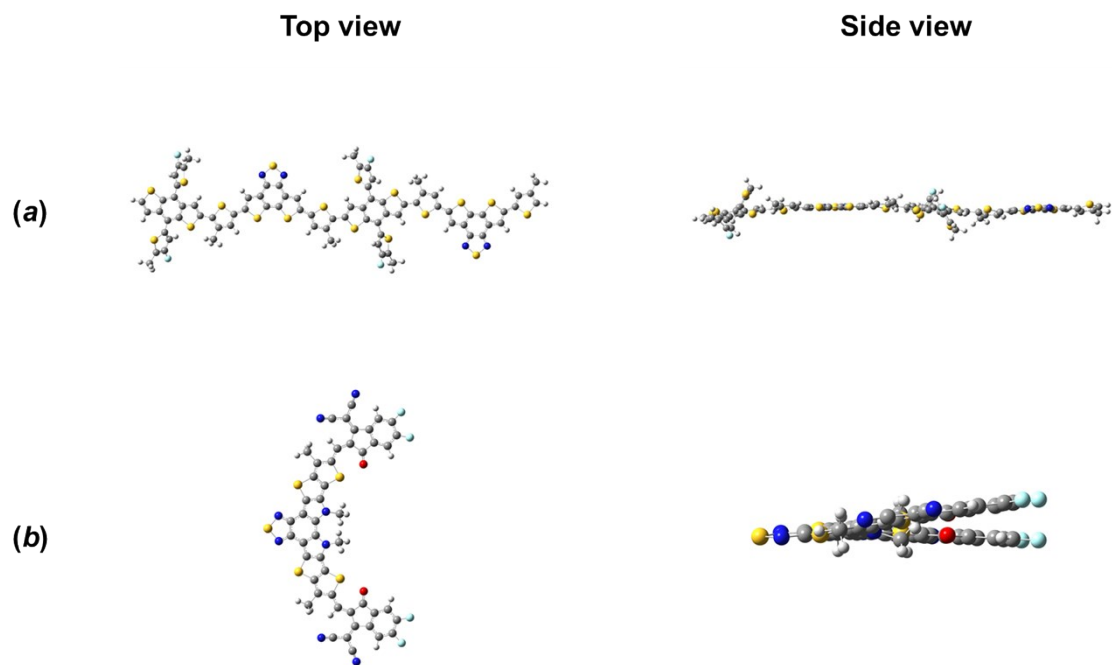
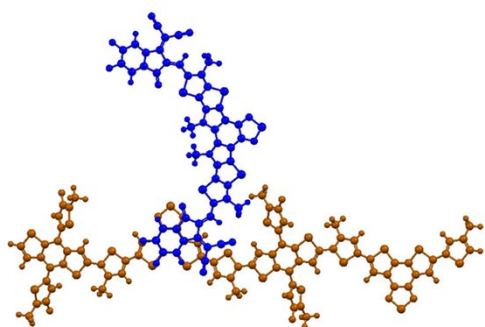


Figure S3. Optimized ground geometries for (a) two repeating units of D18 and (b) Y6 where alkyl groups are all replaced by methyl.

Top view



Side view

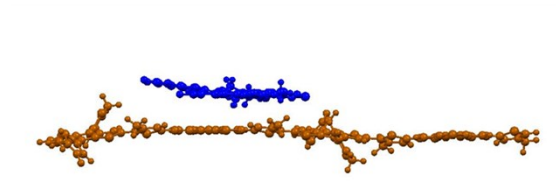


Figure S4. Initial intermolecular configuration of the D18/Y6 complex.

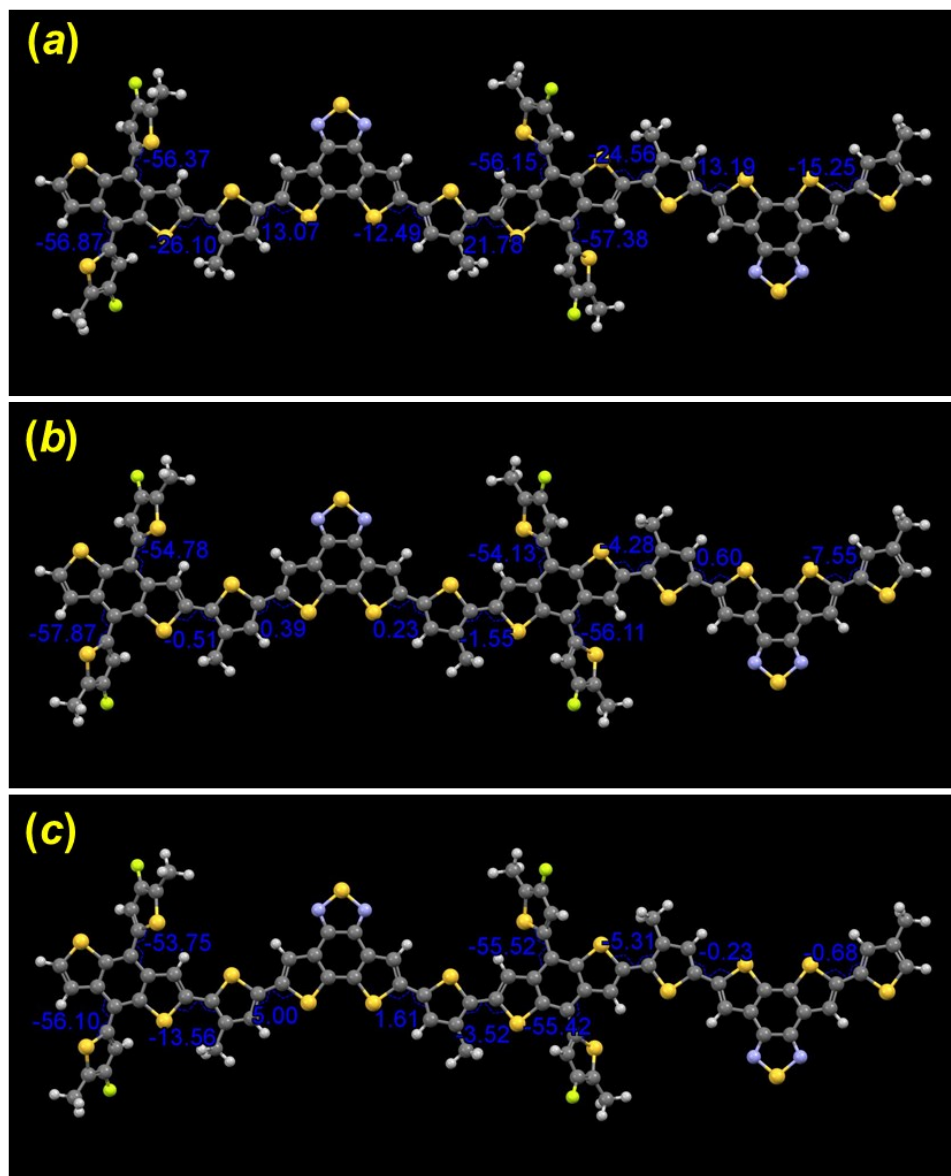


Figure S5. Optimized geometries of the (a) S_0 , (b) S_1 , and (c) cationic states for D18.

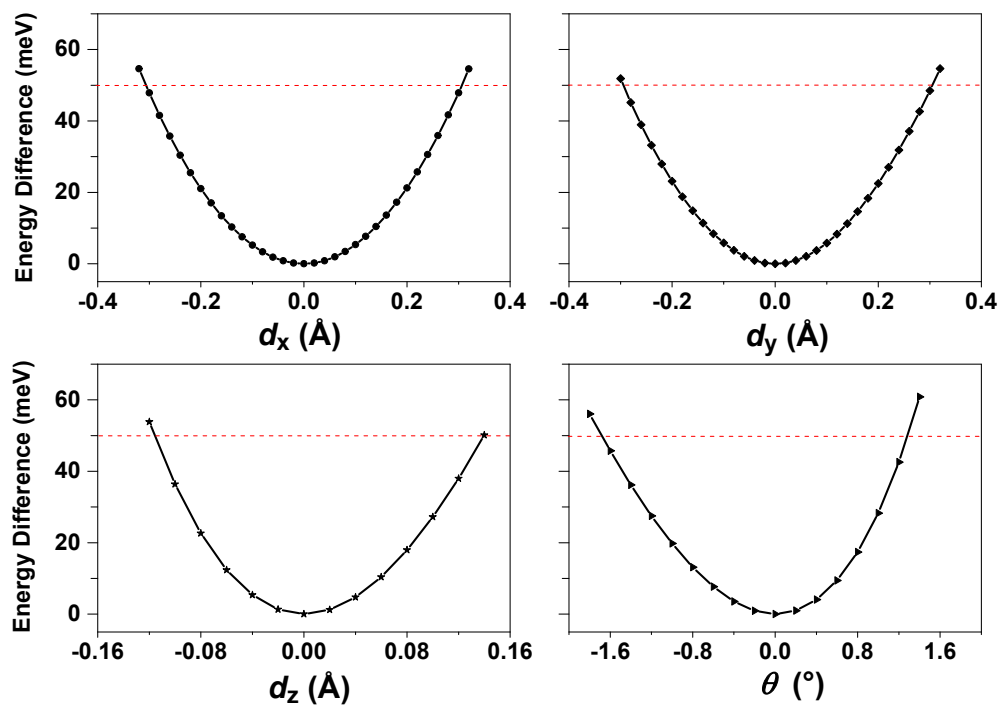


Figure S6. Energy differences between the configurations derived from translation (d_x , d_y , d_z) and rotation (θ) of Y6 and the optimized configuration.

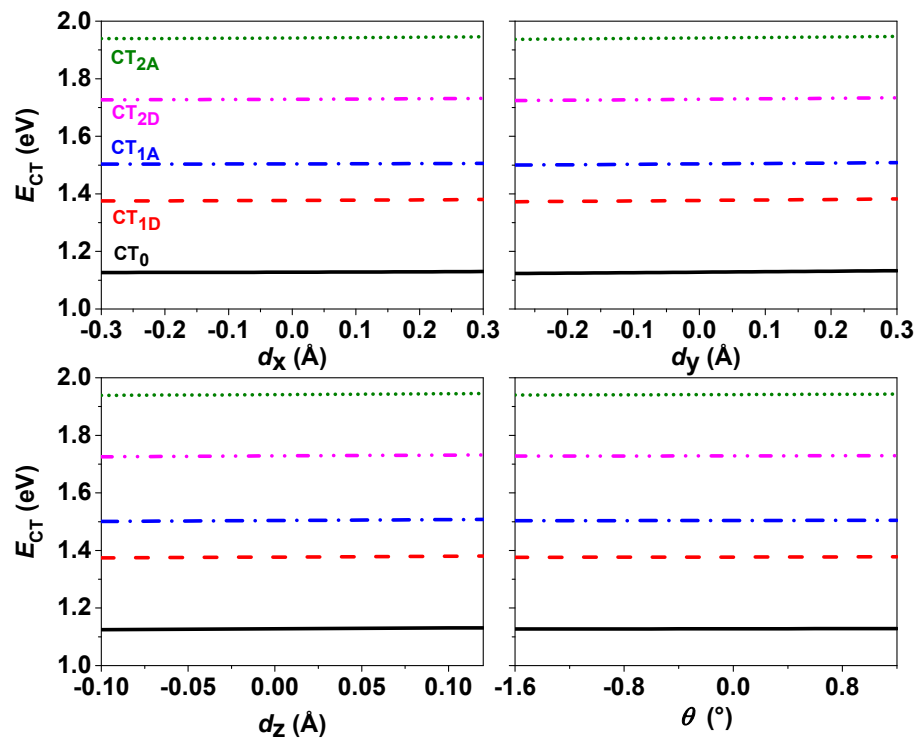


Figure S7. Calculated energies of the CT₀, CT_{1D}, CT_{1A}, CT_{2D} and CT_{2A} states as a function of d_x , d_y , d_z , and θ for the D18/Y6 complex.

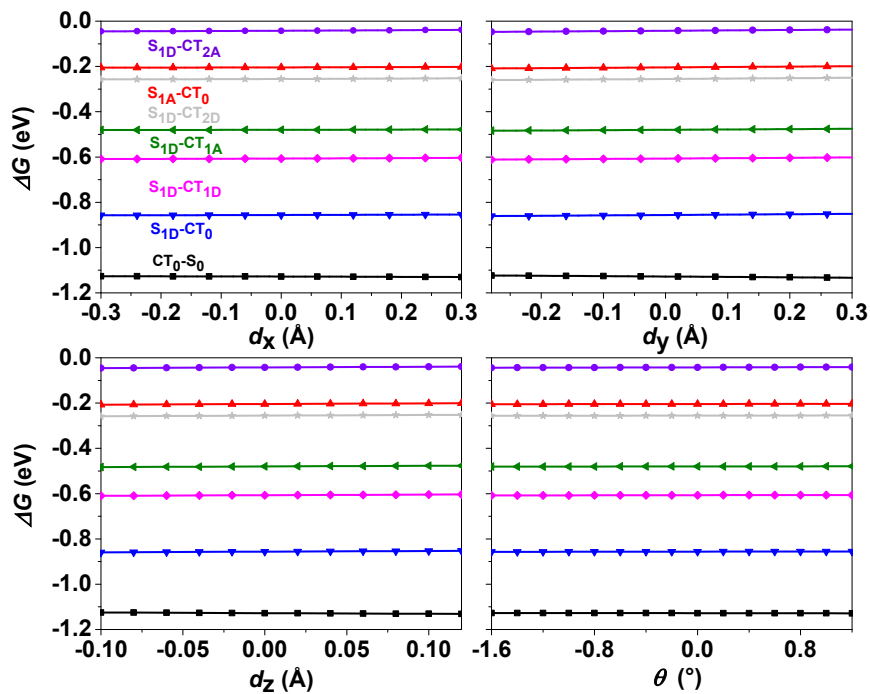


Figure S8. Gibbs free energies for exciton dissociation from the S_1 state of Y6 (S_{1A}) and D18 (S_{1D}) to the CT_0 , CT_{1D} , CT_{1A} , CT_{2D} , and CT_{2A} states, and charge recombination from the CT_0 to S_0 state as a function of d_x , d_y , d_z , and θ for the D18/Y6 complex.

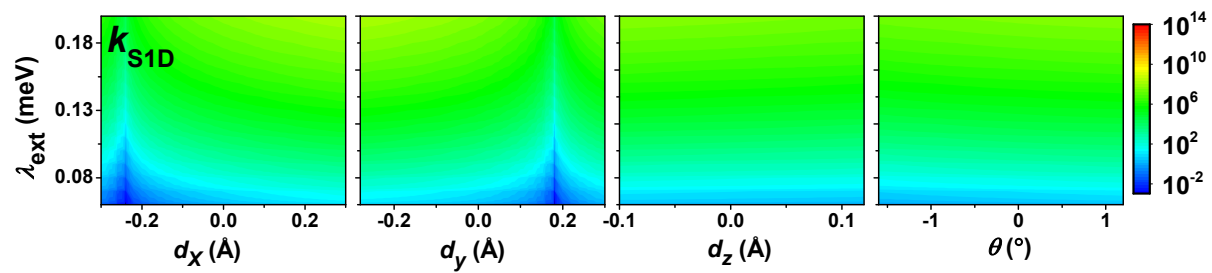


Figure S9. Evolution of the rates (s^{-1}) for exciton dissociation from the S_1 state of D18 to CT_0

(k_{S1D}) as a function of d_x , d_y , d_z , and θ for the D18/Y6 complex.